

Time-Dependent CP Asymmetries in $B^0 \rightarrow K_S^0 \pi^0 \gamma$ Transitions

Y. Ushiroda,⁷ K. Sumisawa,⁷ K. Abe,⁷ K. Abe,⁴¹ I. Adachi,⁷ H. Aihara,⁴³ D. Anipko,¹ K. Arinstein,¹
 A. M. Bakich,³⁹ E. Barberio,¹⁹ M. Barbero,⁶ A. Bay,¹⁷ I. Bedny,¹ K. Belous,¹¹ U. Bitenc,¹³ I. Bizjak,¹³ S. Blyth,²²
 A. Bondar,¹ A. Bozek,²⁵ M. Bračko,^{7,18,13} J. Brodzicka,²⁵ T. E. Browder,⁶ P. Chang,²⁴ Y. Chao,²⁴ A. Chen,²²
 K.-F. Chen,²⁴ W. T. Chen,²² B. G. Cheon,³ R. Chistov,¹² Y. Choi,³⁸ Y. K. Choi,³⁸ S. Cole,³⁹ J. Dalseno,¹⁹
 M. Dash,⁴⁷ S. Eidelman,¹ N. Gabyshev,¹ T. Gershon,⁷ A. Go,²² B. Golob,^{49,13} H. Ha,¹⁵ J. Haba,⁷ K. Hara,²⁰
 M. Hazumi,⁷ D. Heffernan,²⁹ T. Higuchi,⁷ Y. Hoshi,⁴¹ S. Hou,²² W.-S. Hou,²⁴ T. Iijima,²⁰ K. Ikado,²⁰ K. Inami,²⁰
 A. Ishikawa,⁴³ H. Ishino,⁴⁴ R. Itoh,⁷ M. Iwasaki,⁴³ Y. Iwasaki,⁷ J. H. Kang,⁴⁸ N. Katayama,⁷ H. Kawai,²
 T. Kawasaki,²⁷ H. R. Khan,⁴⁴ H. Kichimi,⁷ H. J. Kim,¹⁶ Y. J. Kim,⁵ K. Kinoshita,⁴ P. Krizan,^{49,13} R. Kulasiri,⁴
 R. Kumar,³⁰ A. Kuzmin,¹ Y.-J. Kwon,⁴⁸ M. J. Lee,³⁶ S. E. Lee,³⁶ T. Lesiak,²⁵ A. Limosani,⁷ S.-W. Lin,²⁴
 F. Mandl,¹⁰ D. Marlow,³² T. Matsumoto,⁴⁵ A. Matyja,²⁵ S. McOnie,³⁹ K. Miyabayashi,²¹ H. Miyake,²⁹ H. Miyata,²⁷
 Y. Miyazaki,²⁰ R. Mizuk,¹² G. R. Moloney,¹⁹ T. Mori,²⁰ E. Nakano,²⁸ M. Nakao,⁷ H. Nakazawa,⁷ Z. Natkaniec,²⁵
 S. Nishida,⁷ O. Nitoh,⁴⁶ S. Noguchi,²¹ S. Ogawa,⁴⁰ T. Ohshima,²⁰ S. Okuno,¹⁴ Y. Onuki,³³ H. Ozaki,⁷ P. Pakhlov,¹²
 C. W. Park,³⁸ H. Park,¹⁶ L. S. Peak,³⁹ R. Pestotnik,¹³ L. E. Piilonen,⁴⁷ Y. Sakai,⁷ N. Satoyama,³⁷ T. Schietinger,¹⁷
 O. Schneider,¹⁷ J. Schümann,²³ A. J. Schwartz,⁴ R. Seidl,^{8,33} K. Senyo,²⁰ M. E. Seviar,¹⁹ M. Shapkin,¹¹
 H. Shibuya,⁴⁰ J. B. Singh,³⁰ A. Somov,⁴ N. Soni,³⁰ M. Starič,¹³ H. Stoeck,³⁹ S. Suzuki,³⁴ S. Y. Suzuki,⁷
 O. Tajima,⁷ F. Takasaki,⁷ K. Tamai,⁷ M. Tanaka,⁷ G. N. Taylor,¹⁹ Y. Teramoto,²⁸ X. C. Tian,³¹ K. Trabelsi,⁶
 T. Tsuboyama,⁷ T. Tsukamoto,⁷ S. Uehara,⁷ K. Ueno,²⁴ S. Uno,⁷ P. Urquijo,¹⁹ Y. Usov,¹ G. Varner,⁶
 K. E. Varvell,³⁹ S. Villa,¹⁷ C. H. Wang,²³ Y. Watanabe,⁴⁴ R. Wedd,¹⁹ E. Won,¹⁵ Q. L. Xie,⁹ B. D. Yabsley,³⁹
 A. Yamaguchi,⁴² Y. Yamashita,²⁶ M. Yamauchi,⁷ L. M. Zhang,³⁵ Z. P. Zhang,³⁵ V. Zhilich,¹ and A. Zupanc¹³

(The Belle Collaboration)

¹*Budker Institute of Nuclear Physics, Novosibirsk*

²*Chiba University, Chiba*

³*Chonnam National University, Kwangju*

⁴*University of Cincinnati, Cincinnati, Ohio 45221*

⁵*The Graduate University for Advanced Studies, Hayama, Japan*

⁶*University of Hawaii, Honolulu, Hawaii 96822*

⁷*High Energy Accelerator Research Organization (KEK), Tsukuba*

⁸*University of Illinois at Urbana-Champaign, Urbana, Illinois 61801*

⁹*Institute of High Energy Physics, Chinese Academy of Sciences, Beijing*

¹⁰*Institute of High Energy Physics, Vienna*

¹¹*Institute of High Energy Physics, Protvino*

¹²*Institute for Theoretical and Experimental Physics, Moscow*

¹³*J. Stefan Institute, Ljubljana*

¹⁴*Kanagawa University, Yokohama*

¹⁵*Korea University, Seoul*

¹⁶*Kyungpook National University, Taegu*

¹⁷*Swiss Federal Institute of Technology of Lausanne, EPFL, Lausanne*

¹⁸*University of Maribor, Maribor*

¹⁹*University of Melbourne, Victoria*

²⁰*Nagoya University, Nagoya*

²¹*Nara Women's University, Nara*

²²*National Central University, Chung-li*

²³*National United University, Miao Li*

²⁴*Department of Physics, National Taiwan University, Taipei*

²⁵*H. Niewodniczanski Institute of Nuclear Physics, Krakow*

²⁶*Nippon Dental University, Niigata*

²⁷*Niigata University, Niigata*

²⁸*Osaka City University, Osaka*

²⁹*Osaka University, Osaka*

³⁰*Panjab University, Chandigarh*

³¹*Peking University, Beijing*

³²*Princeton University, Princeton, New Jersey 08544*

³³*RIKEN BNL Research Center, Upton, New York 11973*

³⁴*Saga University, Saga*

³⁵University of Science and Technology of China, Hefei

³⁶Seoul National University, Seoul

³⁷Shinshu University, Nagano

³⁸Sungkyunkwan University, Suwon

³⁹University of Sydney, Sydney NSW

⁴⁰Toho University, Funabashi

⁴¹Tohoku Gakuin University, Tagajo

⁴²Tohoku University, Sendai

⁴³Department of Physics, University of Tokyo, Tokyo

⁴⁴Tokyo Institute of Technology, Tokyo

⁴⁵Tokyo Metropolitan University, Tokyo

⁴⁶Tokyo University of Agriculture and Technology, Tokyo

⁴⁷Virginia Polytechnic Institute and State University, Blacksburg, Virginia 24061

⁴⁸Yonsei University, Seoul

⁴⁹University of Ljubljana, Ljubljana

(Dated: December 2, 2024)

We report measurements of CP violation parameters in $B^0 \rightarrow K_S^0 \pi^0 \gamma$ transitions based on a data sample of $535 \times 10^6 B\bar{B}$ pairs collected with the Belle detector at the KEKB asymmetric-energy e^+e^- collider. One neutral B meson is fully reconstructed in the $B^0 \rightarrow K_S^0 \pi^0 \gamma$ mode. The flavor of the accompanying B meson is identified from its decay products. For a $K_S^0 \pi^0$ invariant mass up to $1.8 \text{ GeV}/c^2$, we obtain $\mathcal{S}_{K_S^0 \pi^0 \gamma} = -0.10 \pm 0.31 \pm 0.07$ and $\mathcal{A}_{K_S^0 \pi^0 \gamma} = -0.20 \pm 0.20 \pm 0.06$. For a $K_S^0 \pi^0$ invariant mass near the $K^{*0}(892)$ resonance, we obtain $\mathcal{S}_{K^{*0} \gamma} = -0.32_{-0.33}^{+0.36} \pm 0.05$ and $\mathcal{A}_{K^{*0} \gamma} = -0.20 \pm 0.24 \pm 0.05$.

PACS numbers: 11.30.Er, 13.25.Hw

The radiative $b \rightarrow s\gamma$ penguin process is sensitive to physics beyond the standard model (SM), and time-dependent CP violation in decays of the type $B^0 \rightarrow f_{CP}\gamma$, where f_{CP} is a CP eigenstate, has drawn much theoretical and experimental interest recently [1, 2, 3, 4, 5, 6, 7, 8]. Within the SM, the photon emitted from a B^0 (\bar{B}^0) meson is predominantly right-handed (left-handed). A flip of photon polarization is suppressed by the quark mass ratio $2m_s/m_b$ [1]. Hence, for $f_{CP} = K^{*0} (\rightarrow K_S^0 \pi^0)$ the SM predicts a small time-dependent CP asymmetry, which arises from the interference between decay amplitudes with and without B^0 - \bar{B}^0 mixing. The same suppression is expected for final states of the type $B^0 \rightarrow P^0 Q^0 \gamma$ [2], where P^0 and Q^0 are any C eigenstate spin-0 neutral particle (e.g. $P^0 = K_S^0$ and $Q^0 = \pi^0$). However, there are estimates predicting an enhancement of the asymmetry up to 0.1 due to strong interactions [3, 4]. For the case of $B^0 \rightarrow K^{*0} (\rightarrow K_S^0 \pi^0) \gamma$, explicit computations [5, 6] support a small asymmetry in the SM. A significant deviation from the small SM expectation could indicate new physics.

Since the time-dependent CP asymmetry is not expected to change significantly as a function of $K_S^0 \pi^0$ invariant mass ($M_{K_S^0 \pi^0}$) [4], we perform two measurements: one for $B^0 \rightarrow K^{*0} (\rightarrow K_S^0 \pi^0) \gamma$ [9] by requiring $M_{K_S^0 \pi^0}$ to lie in the range $0.8 \text{ GeV}/c^2 < M_{K_S^0 \pi^0} < 1.0 \text{ GeV}/c^2$, and the other for the full range of $M_{K_S^0 \pi^0}$ below $1.8 \text{ GeV}/c^2$. For simplicity, we refer to these two analyses as $K^{*0} \gamma$ and $K_S^0 \pi^0 \gamma$, respectively. The measurement for $K^{*0} \gamma$ is theoretically cleaner than the measurement for $K_S^0 \pi^0 \gamma$, but the latter has more statistical power. Similar measure-

ments have been previously reported by both Belle [7] and BABAR [8] based on 275×10^6 and $232 \times 10^6 B\bar{B}$ pairs, respectively. In this Communication, we update the measurements of CP parameters for $B^0 \rightarrow K^{*0} \gamma$ and $B^0 \rightarrow K_S^0 \pi^0 \gamma$ based on a data sample that contains $535 \times 10^6 B\bar{B}$ pairs.

At the KEKB asymmetric-energy e^+e^- (3.5 on 8.0 GeV) collider [10], the $\Upsilon(4S)$ is produced with a Lorentz boost of $\beta\gamma = 0.425$ along the z axis, which is defined as the direction antiparallel to the e^+ beam direction. In the decay chain $\Upsilon(4S) \rightarrow B^0 \bar{B}^0 \rightarrow f_{\text{rec}} f_{\text{tag}}$, where one of the B mesons decays at time t_{rec} to a final state f_{rec} , which is our signal mode, and the other decays at time t_{tag} to a final state f_{tag} that distinguishes between B^0 and \bar{B}^0 , the decay rate has a time dependence given by

$$\mathcal{P}(\Delta t) = \frac{e^{-|\Delta t|/\tau_{B^0}}}{4\tau_{B^0}} \left\{ 1 + q \left[\mathcal{S} \sin(\Delta m_d \Delta t) + \mathcal{A} \cos(\Delta m_d \Delta t) \right] \right\}. \quad (1)$$

Here \mathcal{S} and \mathcal{A} are CP -violation parameters, τ_{B^0} is the B^0 lifetime, Δm_d is the mass difference between the two B^0 mass eigenstates, Δt is the time difference $t_{\text{rec}} - t_{\text{tag}}$, and the b -flavor charge $q = +1$ (-1) when the tagging B meson is a B^0 (\bar{B}^0). Since the B^0 and \bar{B}^0 mesons are approximately at rest in the $\Upsilon(4S)$ center-of-mass system (c.m.s.), Δt can be determined from the displacement in z between the f_{rec} and f_{tag} decay vertices: $\Delta t \simeq (z_{\text{rec}} - z_{\text{tag}})/(\beta\gamma c) \equiv \Delta z/(\beta\gamma c)$.

The Belle detector is a large-solid-angle magnetic spec-

trometer that consists of a silicon vertex detector (SVD), a 50-layer central drift chamber, an array of aerogel threshold Čerenkov counters, a barrel-like arrangement of time-of-flight scintillation counters, and an electromagnetic calorimeter comprised of CsI(Tl) crystals located inside a superconducting solenoid coil that provides a 1.5 T magnetic field. An iron flux-return located outside of the coil is instrumented to detect K_L^0 mesons and to identify muons. The detector is described in detail elsewhere [11]. Two inner detector configurations were used. A 2.0 cm radius beampipe and a three layer silicon vertex detector (SVD1) were used for the first sample of $152 \times 10^6 B\bar{B}$ pairs, while a 1.5 cm radius beampipe, a four layer silicon detector (SVD2) and a small-cell inner drift chamber were used to record the remaining $383 \times 10^6 B\bar{B}$ pairs [12].

For high energy prompt photons, we select an isolated cluster in the ECL that has no corresponding charged track and has the largest energy in the c.m.s. We require $1.4 \text{ GeV} < E_\gamma^{\text{c.m.s.}} < 3.4 \text{ GeV}$. For the selected photon, we also require $E_9/E_{25} > 0.95$, where E_9/E_{25} is the ratio of energies summed in 3×3 and 5×5 arrays of CsI(Tl) crystals around the center of the shower. In order to reduce the background from π^0 or η decays, photons from candidate $\pi^0 \rightarrow \gamma\gamma$ or $\eta \rightarrow \gamma\gamma$ decays are rejected using a likelihood described in detail elsewhere [13]. The polar angle of the photon direction in the laboratory frame is restricted to the barrel region of the ECL ($33^\circ < \theta_\gamma < 128^\circ$) for SVD1 data, but is extended to the end-cap regions ($17^\circ < \theta_\gamma < 150^\circ$) for SVD2 data due to the reduced material in front of the ECL.

Neutral kaons (K_S^0) are reconstructed from two oppositely charged pions that have an invariant mass within $\pm 6 \text{ MeV}/c^2$ (2σ) of the K_S^0 mass [14]. The $\pi^+\pi^-$ vertex is required to be displaced from the interaction point (IP) by a minimum transverse distance of 0.22 cm for high momentum ($> 1.5 \text{ GeV}/c$) candidates and 0.08 cm for those with momentum less than $1.5 \text{ GeV}/c$. The direction of the pion pair momentum must agree with the direction defined by the IP and the two pion vertex point within 0.03 rad for high-momentum candidates, and within 0.1 rad for the remaining candidates. Neutral pions (π^0) are formed from two photons with an invariant mass within $\pm 16 \text{ MeV}/c^2$ (3σ) of the π^0 mass. The photon momenta are then recalculated with a π^0 mass constraint. We then require the momentum of π^0 candidates in the c.m.s. to be greater than $0.3 \text{ GeV}/c$. The $K_S^0\pi^0$ invariant mass, $M_{K_S^0\pi^0}$, is required to be less than $1.8 \text{ GeV}/c^2$.

We also reconstruct $B^0 \rightarrow K^+\pi^-\gamma$ and $B^+ \rightarrow K_S^0\pi^+\gamma$ candidates as control samples in a similar way. Charged tracks other than those from K_S^0 are required to originate from the IP (within 5 cm in z and 1.4 cm in r - ϕ); the transverse momentum (p_t) is required to be greater than $0.1 \text{ GeV}/c$. In the $B^+ \rightarrow K_S^0\pi^+\gamma$ sample, we also require that the π^+ candidate is not positively identified as any other particle species (K^+ , p^+ , e^+ and μ^+). In

the $B^0 \rightarrow K^+\pi^-\gamma$ sample, the K^+ candidate is selected from charged tracks identified as kaons, and the π^- candidate from the rest of tracks.

The $B^0 \rightarrow K_S^0\pi^0\gamma$ and $B^+ \rightarrow K_S^0\pi^+\gamma$ modes are reconstructed simultaneously and a single candidate is selected from possible multiple candidates amongst the two modes in order to reduce the cross-feed background from $B^+ \rightarrow K_S^0\pi^+\gamma$ in $B^0 \rightarrow K_S^0\pi^0\gamma$, where a π^0 is selected instead of the π^+ . The best candidate selection is based on a likelihood ratio \mathcal{R} calculated from likelihood variables for signal (\mathcal{L}_{sig}) and background (\mathcal{L}_{bkg}) as $\mathcal{R} \equiv \mathcal{L}_{sig}/(\mathcal{L}_{sig} + \mathcal{L}_{bkg})$, where the likelihood variables are obtained from a Fisher discriminant \mathcal{F} [15], which uses the modified Fox-Wolfram moments [16] as discriminating variables. Hereafter, we denote the likelihood ratio with the likelihood variable name in parentheses, as $\mathcal{R}(\mathcal{F})$ in this case. We select the candidate that has the largest $\mathcal{R}(\mathcal{F})$. We form two kinematic variables: the energy difference $\Delta E \equiv E_B^{\text{c.m.s.}} - E_{\text{beam}}^{\text{c.m.s.}}$ and the beam-energy constrained mass $M_{bc} \equiv \sqrt{(E_{\text{beam}}^{\text{c.m.s.}})^2 - (p_B^{\text{c.m.s.}})^2}$, where $E_{\text{beam}}^{\text{c.m.s.}}$ is the beam energy, and $E_B^{\text{c.m.s.}}$ and $p_B^{\text{c.m.s.}}$ are the energy and the momentum of the candidate in the c.m.s. The signal region in ΔE and M_{bc} , which is used for the measurements of CP -violating parameters, is defined as $-0.2 \text{ GeV} < \Delta E < 0.1 \text{ GeV}$ and $5.27 \text{ GeV}/c^2 < M_{bc} < 5.29 \text{ GeV}/c^2$. In order to determine the ΔE - M_{bc} dependent signal fraction, a larger fitting region, $-0.3 \text{ GeV} < \Delta E < 0.5 \text{ GeV}$ and $5.2 \text{ GeV}/c^2 < M_{bc}$ is used.

In order to suppress the background contribution from continuum light quark pair production processes ($e^+e^- \rightarrow q\bar{q}$ with $q = u, d, s, c$), which we hereafter refer to as $q\bar{q}$, we form another likelihood ratio $\mathcal{R}(\mathcal{F}, \cos\theta_B, \cos\theta_H)$ by combining \mathcal{F} with $\cos\theta_B$ and $\cos\theta_H$, where θ_B is the polar angle of the B meson candidate momentum in the c.m.s. and θ_H is the helicity angle defined as the kaon momentum direction with respect to the opposite of the B momentum in the K - π rest frame. The helicity distributions for signal and background are determined from the $B^0 \rightarrow K^+\pi^-\gamma$ sample for three mass regions: $0.8 \text{ GeV}/c^2 < M_{K\pi} < 1.0 \text{ GeV}/c^2$ (MR1), $1.3 \text{ GeV}/c^2 < M_{K\pi} < 1.55 \text{ GeV}/c^2$ (MR2), and the remaining range up to $1.8 \text{ GeV}/c^2$ (MR3). The difference of background distributions in $B^0 \rightarrow K^+\pi^-\gamma$ and $B^0 \rightarrow K_S^0\pi^0\gamma$ decay modes is corrected using sideband data samples. In addition, a helicity dependent efficiency correction is applied. Specific $\mathcal{R}(\mathcal{F}, \cos\theta_B, \cos\theta_H)$ selection criteria are applied depending on both the mass region and the flavor tagging information. Background contributions from B decays, which are considerably smaller than $q\bar{q}$, are dominated by cross-feed from other radiative B decays.

The b -flavor of the accompanying B meson is identified from inclusive properties of particles that are not associated with the reconstructed signal decay. The algorithm for flavor tagging is described in detail elsewhere [17]. We

use two parameters, q defined in Eq. (1) and r , to represent the tagging information. The parameter r is an event-by-event flavor-tagging quality factor that ranges from 0 to 1: $r = 0$ when there is no flavor discrimination and $r = 1$ when the flavor assignment is unambiguous. The value of r is determined by using Monte Carlo (MC) and is only used to sort data into seven r intervals. Events with $r > 0.1$ are sorted into six r intervals. The wrong tag fraction w and the difference Δw in w between the B^0 and \overline{B}^0 decays are determined for each of the six r intervals from high-statistics control samples of semileptonic and hadronic $b \rightarrow c$ decays. If r is less than or equal to 0.1, we set w to 0.5, and therefore the accompanying B meson does not provide tagging information in this case.

The vertex position of the signal-side decay of $B^0 \rightarrow K_S^0 \pi^0 \gamma$ position of the signal-side decay of $B^0 \rightarrow K_S^0 \pi^0 \gamma$ and $B^+ \rightarrow K_S^0 \pi^+ \gamma$ is reconstructed from the K_S^0 trajectory with a constraint on the IP; the IP profile ($\sigma_x \simeq 100 \mu\text{m}$, $\sigma_y \simeq 5 \mu\text{m}$) is smeared by the finite B flight length in the plane perpendicular to the z axis. The K_S^0 vertex is displaced from the B vertex and often lies outside of the SVD. In this case, the vertex resolution is not good enough for a time-dependent CP asymmetry measurement. Therefore, both pions from the K_S^0 decay are required to have enough hits in the SVD: at least one layer with hits on both the z and r - ϕ sides and at least one additional hit in the z side of the other layers for SVD1, and at least two layers with hits on both sides for SVD2. The other (tag-side) B vertex is determined from well reconstructed tracks that are not assigned to the signal side. A constraint to the IP profile is also imposed.

After all the selections are applied, we obtain 4078 candidates in the ΔE - M_{bc} fit region, of which 406 are in the signal box. We perform an unbinned maximum likelihood (UML) fit to the ΔE - M_{bc} distribution in order to resolve signal, $B\overline{B}$ background and $q\overline{q}$ background components. The signal probability density function (PDF) is obtained from MC. We use a two-dimensional histogram of MC simulated data, for which the peak position and the width are corrected to account for differences between data and simulation using the $B^0 \rightarrow K^+ \pi^- \gamma$ control sample. The two-dimensional PDF for $B\overline{B}$ background is obtained from MC. For $q\overline{q}$ background, we use the product of two one-dimensional PDFs: the ARGUS parameterization [18] for M_{bc} and a second order polynomial for ΔE . Five parameters, which are the signal fraction, the $B\overline{B}$ background fraction, ARGUS shape parameter α , and two polynomial coefficients (c_1 , c_2), are the free parameters in the fit.

We first fit the entire $M_{K_S^0 \pi^0}$ region, and then fit the MR1, MR2 and MR3 mass regions separately with the three background shape parameters (α , c_1 and c_2) fixed at the values obtained from the fit to the full range. Figure 1 shows a ΔE (M_{bc}) projection of the fit result

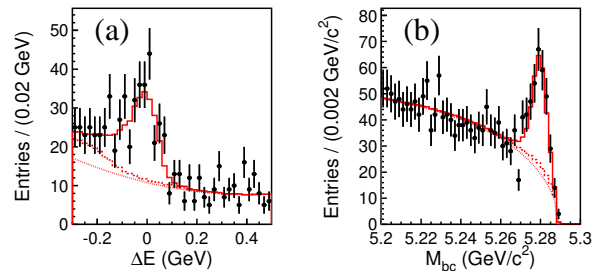


FIG. 1: (a) ΔE distribution within the M_{bc} signal slice and (b) M_{bc} distribution within the ΔE signal slice for the whole $M_{K_S^0 \pi^0}$ region. Points with error bars are measured data. The solid curves show the fit results. The dotted curves show the $q\overline{q}$ background contributions, while the dashed curves show the sum of $q\overline{q}$ and $B\overline{B}$ background contributions.

in the M_{bc} (ΔE) signal slice for the entire $M_{K_S^0 \pi^0}$ region. For the MR1, MR2, and MR3 samples, we find 112.5 ± 12.0 , 28.7 ± 7.1 , and 35.2 ± 10.0 signal events, respectively, with signal-to-background ratios (S/N) of 1.91, 0.81, and 0.35. The level of $B\overline{B}$ background is only 7.7 ± 4.2 , 4.1 ± 2.4 , and 5.3 ± 5.2 $B\overline{B}$ events, respectively. As expected, in the K^{*0} mass region the S/N ratio is high.

We determine \mathcal{S} and \mathcal{A} from an UML fit to the observed Δt distribution. The PDF expected for the signal distribution, $\mathcal{P}_{\text{sig}}(\Delta t; \mathcal{S}, \mathcal{A}, q, w, \Delta w)$, is given by the time-dependent decay rate [Eq. (1)], modified to incorporate the effect of incorrect flavor assignment; the parameters τ_{B^0} and Δm_d are fixed at their world-average values [14]. The distribution is then convolved with the proper-time interval resolution function R_{sig} , which takes into account the finite vertex resolution. The parameterization of R_{sig} is the same as that in the previous measurement [7], while the parameter values are updated for the whole dataset. The PDF for $B\overline{B}$ background events ($\mathcal{P}_{B\overline{B}}$) is modeled in the same way as signal, but with different lifetime and CP -violating parameters, while the resolution function $R_{B\overline{B}}$ is the same as R_{sig} . The effective lifetime of $B\overline{B}$ background is obtained from a fit to the MC sample; the result is 1.356 ± 0.045 ps. The background is assumed to have no CP asymmetry; possible deviations from this assumption ($\mathcal{S} = \pm 0.2$ and $\mathcal{A} = \pm 0.2$) are taken into account in the systematic error.

The PDF for $q\overline{q}$ background events, $\mathcal{P}_{q\overline{q}}$, is modeled as a sum of exponential and prompt components, and is convolved with a double Gaussian which represents the resolution function $R_{q\overline{q}}$. All parameters in $\mathcal{P}_{q\overline{q}}$ and $R_{q\overline{q}}$ are determined by a fit to the Δt distribution of a background-enhanced sample in the ΔE - M_{bc} sideband region.

For each event, the following likelihood function is eval-

uated:

$$\begin{aligned}
P_i = & (1 - f_{\text{ol}}) \int_{-\infty}^{+\infty} \left[f_{\text{sig}} \mathcal{P}_{\text{sig}}(\Delta t') R_{\text{sig}}(\Delta t_i - \Delta t') \right. \\
& + f_{B\bar{B}} \mathcal{P}_{B\bar{B}}(\Delta t') R_{B\bar{B}}(\Delta t_i - \Delta t') \\
& + (1 - f_{\text{sig}} - f_{B\bar{B}}) \mathcal{P}_{q\bar{q}}(\Delta t') R_{q\bar{q}}(\Delta t_i - \Delta t') \left. \right] d(\Delta t') \\
& + f_{\text{ol}} P_{\text{ol}}(\Delta t_i),
\end{aligned} \tag{2}$$

where P_{ol} is a Gaussian function that represents a small outlier component with fraction f_{ol} [19]. The probability of signal (f_{sig}) and background ($f_{B\bar{B}}$) are calculated on an event-by-event basis using the results of the two-dimensional ΔE - M_{bc} fit, and are then multiplied by a factor that depends on the flavor tagging bin r . The r distributions of signal and $q\bar{q}$ background events are estimated by repeating the ΔE - M_{bc} fit procedure for each r interval with the three background shape parameters fixed to the full range result. The $B\bar{B}$ background distribution is estimated from MC since the number of $B\bar{B}$ background events in data is limited.

The only free parameters in the CP fit to $B^0 \rightarrow K_S^0 \pi^0 \gamma$ are $\mathcal{S}_{K_S^0 \pi^0 \gamma}$ and $\mathcal{A}_{K_S^0 \pi^0 \gamma}$, which are determined by maximizing the likelihood function $L = \prod_i P_i(\Delta t_i; \mathcal{S}, \mathcal{A})$, where the product is over all events. We obtain

$$\mathcal{S}_{K_S^0 \pi^0 \gamma} = -0.10 \pm 0.31(\text{stat}) \pm 0.07(\text{syst}), \tag{3}$$

$$\mathcal{A}_{K_S^0 \pi^0 \gamma} = -0.20 \pm 0.20(\text{stat}) \pm 0.06(\text{syst}), \tag{4}$$

where the systematic errors are obtained as discussed below. We define the raw asymmetry in each Δt bin by $(N_{q=+1} - N_{q=-1}) / (N_{q=+1} + N_{q=-1})$, where $N_{q=+1}$ (-1) is the number of observed candidates with $q = +1$ (-1). Figure 2 shows the Δt distributions of the events with $0.5 < r \leq 1.0$ for $q = +1$ and $q = -1$ and the raw asymmetry.

We perform the following fits to confirm the validity of our procedure: a B^+ lifetime fit for the $B^+ \rightarrow K_S^0 \pi^+ \gamma$ sample gives 1.49 ± 0.10 ps, which is consistent with the nominal B^+ lifetime [14]; a B^0 lifetime fit for the $B^0 \rightarrow K_S^0 \pi^0 \gamma$ sample gives $1.53_{-0.17}^{+0.19}$ ps, which is consistent with the nominal B^0 lifetime [14]; and a CP asymmetry fit for the $B^+ \rightarrow K_S^0 \pi^+ \gamma$ sample gives an asymmetry consistent with zero ($\mathcal{S} = 0.20 \pm 0.18$, $\mathcal{A} = 0.05 \pm 0.11$). This is expected since the charged decay is completely flavor specific regardless of the photon polarization. A fit to MR1 data gives $\mathcal{S}_{K^* \pi \gamma} = -0.32_{-0.33}^{+0.36}(\text{stat}) \pm 0.05(\text{syst})$, $\mathcal{A}_{K^* \pi \gamma} = -0.20 \pm 0.24(\text{stat}) \pm 0.05(\text{syst})$. A fit to non-MR1 data gives $\mathcal{S} = +0.50 \pm 0.61(\text{stat}) \pm 0.29(\text{syst})$ and $\mathcal{A} = -0.20 \pm 0.37(\text{stat}) \pm 0.13(\text{syst})$. These results are consistent with those from the full $M_{K_S^0 \pi^0}$ sample.

We evaluate systematic uncertainties in the following categories by fitting the data with each fixed parameter shifted by its error: uncertainties from physics parameters such as Δm_d , τ_{B^0} , effective lifetime and CP asymmetry of $B\bar{B}$ background, uncertainties in the knowledge

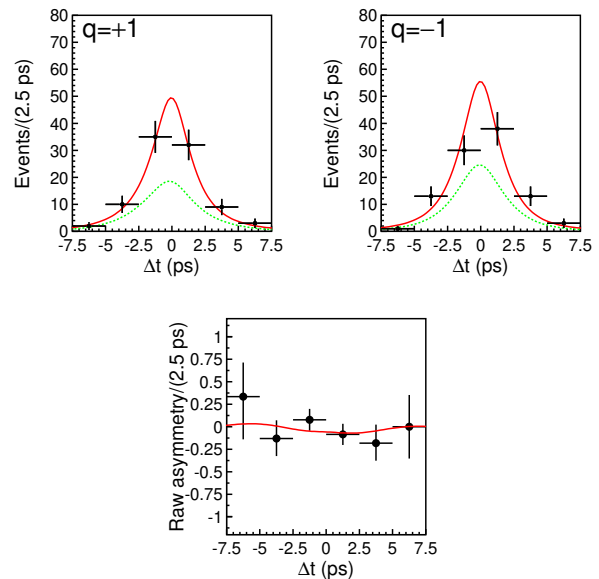


FIG. 2: (Top) Proper time distributions for $B^0 \rightarrow K_S^0 \pi^0 \gamma$ for $q = +1$ (left) and $q = -1$ (right) with $0.5 < r \leq 1.0$. The solid curve shows the total and dashed curve shows the signal component. (Bottom) Asymmetry in each Δt bin with $0.5 < r \leq 1.0$. The solid curve shows the result of the UML fit.

of $q\bar{q}$ background Δt PDF, uncertainties in the flavor tagging, uncertainties in the signal and background fractions, uncertainties in the resolution functions. A possible bias in the fit is checked by fitting a large MC sample. The fit result is consistent with the input value within the statistical error. We quote this statistical error as the possible fit bias. Uncertainty due to the vertex reconstruction is estimated by using the $B^0 \rightarrow J/\psi K_S^0$ control sample, where the tracks from J/ψ are ignored for the study of the signal side vertex reconstruction using the K_S^0 trajectory. The effect of SVD misalignment is estimated by artificially displacing the SVD sensors in a random manner; the standard deviation of these shifts and rotations are $15 \mu\text{m}$ and 0.15 mrad , respectively. Effects of tag-side interference [20] are estimated using $B \rightarrow D^* \ell \nu$. The dominant systematic contributions on \mathcal{S} are from the uncertainties in the signal and background fraction and the resolution function. The systematic error on \mathcal{A} is dominated by the tag-side interference. All these contributions to the systematic errors are summed in quadrature to give 0.07, 0.05 and 0.29 for \mathcal{S} and 0.06, 0.05 and 0.13 for \mathcal{A} for the full $M_{K_S^0 \pi^0}$, MR1 and non-MR1 samples, respectively.

Ensemble tests are carried out with MC pseudo-experiments using the values of \mathcal{S} and \mathcal{A} obtained by the fit as the input parameters. From 10,000 pseudo-experiments, we find that the statistical errors obtained in our measurement are within expectations.

In summary, we have performed a measure-

ment of the time-dependent CP asymmetry in the decay $B^0 \rightarrow K_S^0 \pi^0 \gamma$ with $K_S^0 \pi^0$ invariant mass up to $1.8 \text{ GeV}/c^2$, based on a sample of $535 \times 10^6 B\bar{B}$ pairs. We obtain CP -violation parameters $\mathcal{S}_{K_S^0 \pi^0 \gamma} = -0.10 \pm 0.31(\text{stat}) \pm 0.07(\text{syst})$ and $\mathcal{A}_{K_S^0 \pi^0 \gamma} = -0.20 \pm 0.20(\text{stat}) \pm 0.06(\text{syst})$ for the full $K_S^0 \pi^0$ invariant mass region, and $\mathcal{S}_{K^{*0} \gamma} = -0.32_{-0.33}^{+0.36}(\text{stat}) \pm 0.05(\text{syst})$ and $\mathcal{A}_{K^{*0} \gamma} = -0.20 \pm 0.24(\text{stat}) \pm 0.05(\text{syst})$ for the mass region around $K^{*0}(892)$. This measurement supersedes our previous measurement [7]. With the present statistics, we do not find any significant CP asymmetry and therefore no indication of new physics from right-handed currents.

We thank the KEKB group for excellent operation of the accelerator, the KEK cryogenics group for efficient solenoid operations, and the KEK computer group and the NII for valuable computing and Super-SINET network support. We acknowledge support from MEXT and JSPS (Japan); ARC and DEST (Australia); NSFC and KIP of CAS (China); DST (India); MOEHRD, KOSEF and KRF (Korea); KBN (Poland); MIST (Russia); ARRS (Slovenia); SNSF (Switzerland); NSC and MOE (Taiwan); and DOE (USA).

REFERENCES

- [1] D. Atwood, M. Gronau and A. Soni, Phys. Rev. Lett. **79**, 185 (1997).
- [2] D. Atwood, T. Gershon, M. Hazumi and A. Soni, Phys. Rev. D **71**, 076003 (2005).
- [3] B. Grinstein, Y. Grossman, Z. Ligeti and D. Pirjol, Phys. Rev. D **71**, 011504 (2005).
- [4] B. Grinstein and D. Pirjol, Phys. Rev. D **73**, 014013 (2006).
- [5] M. Matsumori and A. I. Sanda, Phys. Rev. D **73**, 114022 (2006).
- [6] P. Ball and R. Zwicky, arXiv:hep-ph/0609037.
- [7] Belle Collaboration, Y. Ushiroda *et al.*, Phys. Rev. Lett. **94**, 231601 (2005).
- [8] BABAR Collaboration, B. Aubert *et al.*, Phys. Rev. D **72**, 051103 (2005).
- [9] All decay modes include the charge conjugate, unless otherwise stated.
- [10] S. Kurokawa and E. Kikutani, Nucl. Instr. and Meth. A **499**, 1 (2003).
- [11] Belle Collaboration, A. Abashian *et al.*, Nucl. Instr. and Meth. A **479**, 117 (2002).
- [12] Z. Natkaniec *et al.* (Belle SVD2 Group), Nucl. Instr. and Meth. A **560**, 1 (2006).
- [13] Belle Collaboration, P. Koppenburg *et al.*, Phys. Rev. Lett. **93**, 061803 (2004).
- [14] Particle Data Group, W.-M. Yao *et al.*, Journal of Physics G **33**, 1 (2006).
- [15] R. A. Fisher, Annals Eugen. **7**, 179 (1936).
- [16] Belle Collaboration, K. Abe *et al.*, Phys. Rev. Lett. **91**, 261801 (2003).
- [17] H. Kakuno, K. Hara *et al.*, Nucl. Instr. and Meth. A **533**, 516 (2004).
- [18] ARGUS Collaboration, H. Albrecht *et al.*, Phys. Lett. B **241**, 278 (1990).
- [19] Belle Collaboration, K. Abe *et al.*, Phys. Rev. D **71**, 072003 (2005); H. Tajima *et al.*, Nucl. Instr. and Meth. A **533**, 370 (2004).
- [20] O. Long, M. Baak, R. N. Cahn and D. Kirkby, Phys. Rev. D **68**, 034010 (2003).